International Communications in Heat and Mass Transfer 156 (2024) 107674

Contents lists available at ScienceDirect

International Communications in Heat and Mass Transfer

journal homepage: www.elsevier.com/locate/ichmt

# Characteristic analysis and performance investigation of a new inclined-flowsegmented miniature-channel regenerator

Minjie Yu, Lei Xu, Haichuan Cui, Zhichun Liu, Wei Liu *

*School of Energy and Power Engineering, Huazhong University of Science and Technology, Wuhan 430074, China*

ARTICLE INFO

*Keywords:*
Inclined-flow
Stirling regenerator
Miniature-channel
Thermal and flow characteristics
Overall output performance

ABSTRACT

Regenerator characteristics play a pivotal role in shaping the overall performance of Stirling engines. To refine the thermal and flow characteristics of regenerators and elevating the overall output efficiency of engines, this study introduces an innovative design concept for inclined-flow regenerators, where the gas flow direction is inclined to the matrix surface. A novel inclined-flow segmented miniature-channel regenerator, incorporating miniature-channel structures, was fabricated on the basis of this concept. A comprehensive investigation, spanning both component and system levels, was undertaken for scrutinizing the localized distribution and dynamic responses of flow and heat transfer within this regenerator, elucidate the mechanisms through which the regenerator influences engine performance, and compare its efficacy with that of cross-flow and parallel-flow regenerators. The findings underscore that the inclined-flow miniature-channel regenerator attains a harmonious equilibrium in thermal and flow characteristics. Equipping engines with this regenerator yields a notable 325% surge in output power and a 127% boost in thermal efficiency compared to cross-flow regenerators. Furthermore, it demonstrates a 3% increase in output power and a 171% enhancement of thermal efficiency than parallel-flow regenerators. These results affirm the feasibility of the presented concept for inclined-flow regenerators and the constructed inclined-flow miniature-channel regenerator in augmenting Stirling engine performance.

## 1. Introduction

As human society continues to advance economically and technologically, there is an ever-increasing demand for energy, coupled with a growing emphasis on environmental protection [1]. However, traditional fossil fuels, aside from being finite in supply, exacerbate global climate and ecological crises due to their widespread utilization [2]. Hence, there is an urgent necessity for the exploration and development of clean, renewable alternative energy sources and the creation of efficient, innovative energy utilization systems [3,4]. With a broad spectrum of energy applicability and high theoretical thermal efficiencies comparable to the Carnot efficiency limit [5], along with the attributes of clean operation, minimal noise, and cost-effective maintenance, the Stirling engine stands out from a crowd of energy conversion systems and holds great promise for the application of renewable energy sources such as solar, geothermal, and biomass energy over a wide temperature range [6,7].

The Stirling engine operates within a closed cycle [8], with its internal working gas circulating through two chambers (compression chamber and expansion chamber), as well as three heat exchangers (heater, regenerator, and cooler) [9]. Among these components, the regenerator plays a pivotal role in ensuring the efficient operation of Stirling engines [10]. Positioned between the hot and cold ends of engines, the regenerator matrix alternately absorbs and releases heat from the gas. Therefore, it functions like a thermal sponge within the engine, which can substantially diminish the quantity of heat absorbed from the heat source simultaneously sustaining a noteworthy temperature differential between the hot and cold ends, consequently resulting in a substantial enhancement of the overall system thermal efficiency [11]. During the engine's operation, the thermal and flow characteristics within the regenerator exert a significant influence on the overall output performance of engines. Ideally, a regenerator should exhibit optimal heat transfer performance while minimizing flow resistance, as this feature minimizes thermal and power losses within the engine, resulting in peak overall system performance [12]. However, in practice, achieving simultaneous maximization of heat transfer and flow performance in a regenerator poses a considerable challenge [13]. Improving one aspect often comes at the expense of the other. Currently, the most

* Corresponding author.
*E-mail address:* w_liu@hust.edu.cn (W. Liu).

https://doi.org/10.1016/j.icheatmasstransfer.2024.107674

prevalent types of regenerators employed in Stirling engines fall into two categories: cross-flow [14] and parallel-flow [15] regenerators. Cross-flow regenerators feature a matrix surface characterized by numerous flow stagnation zones perpendicular to the direction of gas flow. Additionally, as the gas flows laterally around the matrix, it experiences significant flow separation. This intensifies the gas-solid interaction, resulting in high rates of gas-solid convective heat transfer but also substantial flow resistance. In contrast, parallel-flow regenerators facilitate gas flow that is nearly parallel to the matrix surface, with minimal disruption caused by the matrix. As a result, flow resistance is greatly diminished, but the thermal performance decreases significantly as well. In summary, these two types of regenerators approximately represent the two opposite extremes of thermal and flow characteristics. Nevertheless, for a practical regenerator, excessive flow resistance and insufficient heat transfer performance can both lead to a sharp increase in energy losses within the engine, thereby significantly compromising the engine's overall performance.

In pursuit of enhancing the overall performance of the aforementioned two types of regenerators, extensive research efforts have been devoted to exploring the impact of various operational parameters (such as hot and cold source temperature [16], charge pressure [16], and engine speed [17]) and geometric parameters (like hydraulic diameter [18], porosity [19], and regenerator length [20]) on their internal thermal and flow characteristics. Investigation and optimization of these parameters has deepened our comprehension of the gas-matrix convective heat transfer mechanisms in these regenerators and has led to some degree of enhancement in engine performance when these regenerators are integrated. However, due to the specific matrix structures inherent in these two types of regenerators, which dictate the prescribed flow patterns of the working gas, further improvements in regenerator performance through the optimization of operational and local geometric parameters have encountered diminishing returns. There exists an imperative need to introduce a novel optimization approach that can further augment the regenerator's comprehensive thermal and flow performance. A promising solution involves the introduction of a new category of regenerator matrix structures to manipulate the flow patterns of gas within the regenerator, thereby unlocking substantial potential for enhancing both regenerator and engine performance. Considering the interplay between heat transfer and flow characteristics, a configuration of inclined-flow regenerators emerges as a logical pursuit, positioning their matrix structures and internal flow patterns between those of cross-flow and parallel-flow regenerators. These new regenerators feature a matrix surface inclined at a specific angle to the direction of gas flow, resulting in an intermediate level of interaction strength between the gas and the matrix when compared to the first two types of regenerators. Consequently, they are anticipated to exhibit thermal and flow characteristics which fall between those of cross-flow and parallel-flow regenerators. Simultaneously, to achieve a larger surface area and a uniformly distributed flow space with a well-structured design, we incorporated the widely utilized and efficient miniature-channel structure from engineering practice into the regenerator design. Miniature-channel structures are widely recognized in heat transfer [21,22] and storage [23,24] applications due to their advantages of simple, compact, and cost-effective design [25]. In the context of regenerators, miniature-channel structures have, until now, only been applied to parallel-flow regenerators [26,27]. However, because the interaction between the channel surface and the gas within these regenerators is relatively weak (primarily restricted to laminar flow), the heat transfer performance of the regenerator has been significantly limited ($Nu \approx 3$–$7$) [26]. To achieve a well-balanced thermal and flow characteristic within the regenerator, we are pioneering the application of miniature-channel structures to the construction of inclined-flow regenerators.

In addition, the regenerator's investigation can be approached from two distinct levels: the component and system levels. Regenerators are generally treated as individual gas-solid coupled heat transfer components when at the component level. This approach entails an in-depth analysis of the thermal [27–29] and flow [30–32] characteristics exhibited by regenerators with various geometric types and parameters across a range of operational conditions. The ultimate goal is to optimize regenerator parameters to achieve the optimal overall thermal and flow performance. On the other hand, research at system levels involves the amalgamation of regenerators into the broader engine system. From this vantage point, the focus shifts toward investigating the influence of the regenerator's thermal and flow characteristics on the engine's overall output performance [33–35], thereby indicating the direction for optimizing regenerator characteristics [11,16,36]. To evaluate the practical viability of the novel inclined-flow regenerator in engines, this study will integrate analyses by combining these two levels. The investigation will delve into the regenerator's thermal and flow characteristics, aiming to discern its impact on the engine's comprehensive performance under complex oscillating flow conditions.

Therefore, the primary objective of this research is to introduce a new design concept of inclined-flow regenerators with matrix surfaces inclined to the direction of gas flow, and further to construct an inclined-flow miniature-channel regenerator based on the miniature-channel structure. This design approach seeks to obtain superior overall thermal and flow characteristics compared with the cross-flow and parallel-flow regenerator, thus improving the overall output performance of the Stirling engine. The mathematical relationships encompassing key parameters of the engine and regenerator, regenerator's characteristics, and engine's overall output performance were established. These relationships were subjected to rigorous verification through a meticulous comparison of numerical findings with pertinent experimental results. In the following, we analyzed the localized distribution and instantaneous variations of the regenerator's thermal and flow characteristics under oscillating flow conditions, exploring the influence mechanisms of critical regenerator geometric parameters on the comprehensive performance of the regenerator and engine. Finally, through a comparative analysis of the overall output efficacy of Stirling engines integrated with the three types of regenerators, the potential of the design concept of inclined-flow regenerators proposed in this paper and the inclined-flow miniature-channel regenerator constructed based on this concept were demonstrated. In summary, the main innovations of this research include:

(1) The introduction of the novel design strategy of inclined-flow regenerators in which the gas flow direction is inclined to the matrix surface.

(2) For the first time, miniature-channel structure is employed to design the inclined-flow regenerator matrix.

(3) A comprehensive investigation at both the component and system levels into the regenerator's thermal and flow characteristics and engine's overall output performance under complex oscillating flow conditions.

## 2. Regenerator geometric configurations

The inclined-flow miniature-channel regenerator (IMCR), designed based on the miniature-channel structure, is illustrated in Fig. 1. This regenerator features an annular cylindrical configuration, as depicted in Fig. 1 (a). The whole regenerator is divided into $N_r$ equal-length sub-regenerators along the axial direction. Each sub-regenerator comprises several hundred rows of circular miniature channels, each with a diameter of $d_0$, tangentially inclined at an angle of $\beta$. Adjacent sub-regenerators are precisely positioned using locator protrusions and grooves, and the miniature channels within adjacent sub-regenerators are arranged in a mirror-image pattern to ensure axial connectivity in the flow space of regenerators. Considering the periodic distribution of flow channels in the circumferential direction within the regenerator, this study focuses on a computational domain that comprises a single row of miniature channels flanked by two half rows of the miniature channels on each side, as visualized in Fig. 1 (b). The precise alignment

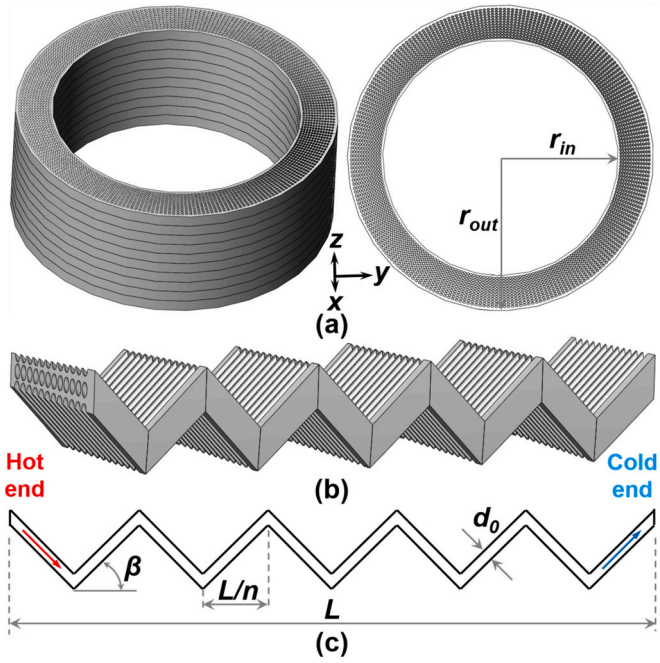


**Fig. 1.** Structures of inclined-flow miniature-channel regenerators.

of miniature channels in adjacent sub-regenerators results in a continuous axial corrugated passage, as depicted in Fig. 1 (c).

In contrast to cross-flow regenerators, the regular and inclined flow spaces within the inclined-flow miniature-channel regenerator significantly suppress flow separation induced by gas flowing around the matrix surface, and eliminate most of the flow stagnation regions. This will minimize the occurrence of pressure surges, thus leading to substantially reduced flow resistance within the regenerator. In contrast to parallel-flow regenerators, the corrugated channel surfaces in this regenerator bring about periodic changes in gas velocity at the peak and valley. This phenomenon directs the gas to sweep across the matrix surface on the opposite side at inclined angles and induces turbulence and local swirling flows, thereby enhancing gas-matrix interactions and promoting cross-layer mixing of the gas. These combined effects contribute to improved uniformity of gas temperature within the regenerator channels, heightened temperature gradients near the matrix surface, and ultimately, an reinforcement in the regenerator's thermal performance.

To ensure the regenerator possesses an adequate thermal mass ratio for efficient heat exchange between the matrix and the gas, it is imperative that the radial interval ($\delta_r$) and the minimum circumferential interval ($\delta_{c,min}$) between channels conform to the minimum thermal penetration depth, $\delta_T$, as delineated below [26]:

$$\delta_r, \delta_{c,min} \geq \delta_T \tag{1}$$

where the minimum thermal penetration depth ($\delta_T$) is defined as the distance over which heat diffuses within the matrix during a single blowing period $t_{blow} = 1/(\pi f)$, and can be calculated using the following expression [26]:

$$\delta_T = \sqrt{\frac{\lambda_s}{\pi f \rho_s c_{p,s}}} \tag{2}$$

where $f$ represents the engine frequency, while $\lambda_s$, $\rho_s$, and $c_{p,s}$ is the thermal conductivity, density, and specific heat capacity of the matrix solid material, respectively.

The inner and outer clearances on each row of channels in the regenerator is set at a constant value of $a = 1$ mm. Consequently, the number of channels per row along the radial direction of the regenerator $N_{per\ row}$ is determined as follows:

$$N_{per\ row} = \frac{r_{out} - r_{in} - 2a}{\delta_r + d_0} \leq \frac{r_{out} - r_{in} - 2a}{\delta_T + d_0} \text{(take the maximum integer)} \tag{3}$$

The number of channel rows $N_{row}$ in the regenerator and the central angle between adjacent channel rows $\theta$ are as follows:

$$N_{row} = \frac{2\pi(r_{in} + a)cos(\beta)}{\delta_{c,min} + d_0} \leq \frac{2\pi(r_{in} + a)cos(\beta)}{\delta_T + d_0} \text{(take the maximum integer)} \tag{4}$$

$$\theta = \frac{360^{\circ}}{N_{row}} \tag{5}$$

Based on the aforementioned geometric constraints, once the engine frequency ($f$), the number of sub-regenerators ($N_r$), the inclined angle of channels ($\beta$), and the channel diameter ($d_0$) are specified, the structure of the regenerator can be determined. Clearly, variations in the geometric parameters $N_r$, $\beta$, and $d_0$ can lead to significant alterations in the flow space structure within the regenerator, potentially exerting a pronounced influence on its thermal and flow characteristics. Therefore, for improving both the regenerator and engine's overall performance, this paper will undertake a parametric study focusing on these three critical geometric parameters. Table 1 gives the primary geometric specification of the inclined-flow miniature-channel regenerators.

## 3. Mathematic methodologies

### 3.1. Governing equation of regenerator models

In this study, helium is employed as the working gas in the Stirling engine. Taking into consideration the gas's viscosity and compressibility, the gas density is determined using the ideal gas equation of state, while other thermo-physical properties are considered as temperature-dependent functions. Driven by the reciprocating motion of pistons, the gas inside the regenerator undergoes periodic transient flow. To minimize axial conductive heat transfer, the regenerator matrix is crafted from stainless steel, chosen for its lower thermal conductivity of about 26 W/(m·K) [16]. Additionally, the segmentation of the regenerator substantially increases the axial contact thermal resistance between adjacent sub-regenerators, further mitigating axial conduction losses. Consequently, this paper considers the heat transfer between gas and matrix, as well as the internal heat conduction within each, but neglects the impact of axial conduction losses on the engine performance. Furthermore, all volumetric forces and heat leakage to the external environment are disregarded. Thereby, the governing equations within the regenerator are as follows [37–39]:

Mass conservation equation:

$$\frac{D\rho_f}{Dt} + \rho_f \nabla \cdot \boldsymbol{u} = 0 \tag{6}$$

Momentum conservation equation:

**Table 1**
Key geometric parameters of inclined-flow miniature-channel regenerators.

| Geometric parameter | Value |
|---|---|
| Regenerator length $L$ | 50 mm |
| Regenerator outer radius $r_{out}$ | 65 mm |
| Regenerator inner radius $r_{in}$ | 50 mm |
| Matrix channel inclined angle $\beta$ | 15–60° |
| Sub-regenerator number $N_r$ | 5–15 |
| Matrix channel diameter $d_0$ | 0.3–1.5 mm |

$$\rho_f \frac{\partial \boldsymbol{u}}{\partial t} + \boldsymbol{u}\cdot\nabla\left(\rho_f \boldsymbol{u}\right) = -\nabla p - \frac{2}{3}\nabla\left[\mu(\nabla\cdot\boldsymbol{u})\right] + \nabla\cdot\left[\mu\left(\nabla\boldsymbol{u} + (\nabla\boldsymbol{u})^T\right)\right] \tag{7}$$

Energy conservation equation for the gas:

$$\rho_f c_{p,f} \frac{DT_f}{Dt} = \nabla\cdot\left(\lambda_f \nabla T_f\right) + \frac{Dp}{Dt} + h\alpha_r\left(T_s - T_f\right) \tag{8}$$

Energy conservation equation for the matrix solid:

$$\rho_s c_{p,s} \frac{\partial T_s}{\partial t} = \nabla\cdot\left(\lambda_s \nabla T_s\right) + h\alpha_r\left(T_f - T_s\right) \tag{9}$$

Ideal gas equation of state for solving the gas density:

$$\rho_f = \frac{p}{R_g T_f} \tag{10}$$

In the equations above, $t$ represents time; $u$, $p$, and $T_f$ refer to the velocity vector, pressure, and temperature of the gas, respectively; $c_{p,f}$, $\rho_f$, $\lambda_f$, $\mu$, and $R_g$ denote the specific heat, density, thermal conductivity, viscosity, and gas constant of the gas, respectively; $T_s$ signifies the temperature of the matrix. $h$ corresponds to the overall gas-solid heat transfer coefficient within the regenerator, and $\alpha_r$ denotes the specific surface area of the matrix, which can be calculated using the following formula:

$$\alpha_r = \frac{4\varphi}{d_h} \tag{11}$$

where $\varphi$ and $d_h$ denote the matrix's porosity and hydraulic diameter, respectively, and they are determined by the following expression:

$$\varphi = 1 - \frac{V_s}{V} \tag{12}$$

$$d_h = \frac{4\varphi V}{A_s} = d_0 \tag{13}$$

where $V_s$ and $V$ represent the matrix volume and regenerator total volume, respectively, while $A_s$ stands for the matrix surface area.

### 3.2. Solution scheme of regenerator models

#### 3.2.1. Boundary conditions

In practical operation of Stirling engines, the pistons inside the engine undergo instantaneous reciprocating motion. This pistons movement induces intricate, periodic oscillations in the gas's physical fields at both ends of the regenerator. To facilitate the numerical solution of the regenerator model, we have derived simplified mathematical expressions for the boundary conditions of the regenerator based on the adiabatic model of Stirling engines [40].

According to the adiabatic model, the mass flow rates of the gas at the hot and cold ends of the regenerator, denoted as $\dot{m}_{kr}$ and $\dot{m}_{rh}$ can be determined. Therefore, the average mass flux of the gas through the regenerator is given by:

$$\dot{m}_r = \frac{\dot{m}_{kr} + \dot{m}_{rh}}{2A_r}\left(\mathrm{kg}/\left(\mathrm{rad}\cdot\mathrm{m}^2\right)\right) \tag{14}$$

where $A_r$ represents the effective flow area of the regenerator, defined as $A_r = \pi\left(r_{out}^2 - r_{in}^2\right)\varphi$. Considering that the units for mass flux are kg/(rad·m$^2$), it can be converted into the ISO standard units by multiplying it by the engine angular velocity $\omega$:

$$\dot{m}_r = \frac{\left(\dot{m}_{kr} + \dot{m}_{rh}\right)\omega}{2A_r}\left(\mathrm{kg}/\left(\mathrm{s}\cdot\mathrm{m}^2\right)\right) \tag{15}$$

Herein, the previously determined average mass flux of the gas through the regenerator serves as the boundary condition at the regenerator's hot end. Additionally, the internal pressure within the engine, denoted as $p_{engine}$, is considered as the boundary condition at the regenerator's cold end:

$$\dot{m}_{r,hot} = \dot{m}_r \tag{16}$$

$$p_{r,cold} = p_{engine} \tag{17}$$

By solving the adiabatic model, a series of discrete values for the regenerator boundary conditions within a cycle can be obtained. These values are then fitted using transcendental functions to derive the boundary conditions at the hot and cold ends of the regenerator as follows:

$$\dot{m}_{r,hot} = \mathrm{e}_1 + \sum_{\mathrm{i}=1}^{8}\left(\mathrm{a}_{1\mathrm{i}} cos(\mathrm{b}_{1\mathrm{i}}\cdot\mathrm{i}\cdot t) + \mathrm{c}_{1\mathrm{i}} sin(\mathrm{d}_{1\mathrm{i}}\cdot\mathrm{i}\cdot t)\right) \tag{18}$$

$$p_{r,cold} = \mathrm{e}_2 + \sum_{\mathrm{i}=1}^{8}\left(\mathrm{a}_{2\mathrm{i}} cos(\mathrm{b}_{2\mathrm{i}}\cdot\mathrm{i}\cdot t) + \mathrm{c}_{2\mathrm{i}} sin(\mathrm{d}_{2\mathrm{i}}\cdot\mathrm{i}\cdot t)\right) \tag{19}$$

where $\mathrm{a}_{1\mathrm{i}}$, $\mathrm{a}_{2\mathrm{i}}$, $\mathrm{b}_{1\mathrm{i}}$, $\mathrm{b}_{2\mathrm{i}}$, $\mathrm{c}_{1\mathrm{i}}$, $\mathrm{c}_{2\mathrm{i}}$, $\mathrm{d}_{1\mathrm{i}}$, $\mathrm{d}_{2\mathrm{i}}$, $\mathrm{e}_1$, and $\mathrm{e}_2$ are the coefficients of the equations.

The engine's hot-end temperature ($T_H$) and cold-end temperature ($T_K$) are defined as 922 K and 288 K, respectively. The temperature of the gas entering the regenerator is equal to that of the corresponding end of the engine, while the outlet temperature is determined through calculations. Two corrugated profiles aligned with the miniature channels are implemented as rotating periodic boundary conditions across the surfaces of the computational domain. Within the miniature channels, the gas-solid interface is treated as a coupled heat-transfer wall with no-slip velocity conditions, while all other matrix surfaces are modeled as adiabatic walls with no-slip boundary conditions.

#### 3.2.2. Solver settings

Guided by the corrugated matrix surface that periodically changes its inclination direction, the gas flow is susceptible to turbulence and local secondary swirling flow phenomena in the channel, especially in the vicinity of the peaks and valleys. Therefore, the Realizable $k$-$\varepsilon$ turbulence model is employed to forecast the flow and heat transfer within the regenerators. This model offers superior predictive accuracy in scenarios with intricate secondary flows and pronounced streamline curvature than the Standard $k$-$\varepsilon$ turbulence model [41]. The SIMPLE algorithm is adopted for pressure-velocity coupling calculations. Second-order upwind schemes are used for spatial discretization of the mass, momentum, and energy equations, while the temporal discretization employs a second-order implicit scheme. Additionally, based on the Courant number method, the time step is chosen as 1/360 of a cycle, which aligns with the reasonable range of time step values matched with grid size for transient problems.

### 3.3. Evaluation of thermal and flow performance for various types of regenerators

Herein, the gas in regenerators with various structures possesses the equal instantaneous mass flow rate. However, caused by disparities in their characteristic dimensions, these regenerators operate at distinct Reynolds numbers (*Re*), a dimensionless parameter that excludes size effects. Consequently, it is not appropriate to quantify the regenerator's pressure drop performance based on the dimensionless resistance coefficient (*Cf*), which also disregards size effects. In this study, a dimensionless parameter, the Euler number (*Eu*), which takes size effects into account, is introduced to characterize the flow resistance performance of the inclined-flow miniature-channel regenerator:

$$Eu = \frac{|\Delta p_r|}{\rho_f u_r^2} \tag{20}$$

where $\Delta p_r$ and $u_r$ represent the pressure drop and the average flow velocity of the gas through the regenerator, respectively.

Furthermore, the overall heat transfer performance within the regenerator is characterized by the regenerator effectiveness $\varepsilon_r$, defined as:

$$\varepsilon_r = \frac{T_h - T_k}{T_H - T_K} \tag{21}$$

where $T_h$ and $T_k$ denote the gas temperature at the hot and cold ends of the regenerator, respectively.

To showcase the feasibility of the inclined-flow miniature-channel regenerators, it is crucial to conduct a comparative assessment of the output performance for engines with this regenerator against that with a cross-flow regenerator and a parallel-flow regenerator under the same operating conditions. Prior to this comparative analysis, it is imperative to acquire the thermal and flow characteristics of the latter two types of regenerators. Herein, the classic stacked woven screen regenerator (SWSR) [42] and parallel miniature-channel regenerator (PMCR) [26] are employed as representatives of cross-flow and parallel-flow regenerators, respectively, and calculate their pressure drop and thermal performance using empirical formulas obtained from experiments or simulations available in the literature. The resistance coefficients (*Cf*) and Nusselt number (*Nu*) for these two regenerators are provided below:

Stacked woven screen regenerator (SWSR) [42]:

$$Cf_c = \frac{129}{Re_h} + 2.91 Re_h^{-0.103} \tag{22}$$

$$Nu_c = \left[1 + 0.99 (Re_h Pr)^{0.66}\right] \varphi^{1.79} \tag{23}$$

Parallel miniature-channel regenerator (PMCR) [26]:

$$Cf_p = \frac{64}{Re_h} \tag{24}$$

$$Nu_p = 1.143 Re_h^{0.2488} \tag{25}$$

In these formulas, *Pr* denotes the gas's Prandtl number. $Re_h$ represents the hydraulic Reynolds number that is determined using the following expression:

$$Re_h = \frac{u_r d_h \rho_f}{\mu} \tag{26}$$

Therefore, the pressure drop of the gas through the aforementioned two types of regenerator is:

$$\Delta p_r = \frac{1}{2} Cf \frac{L}{d_h} \rho_f u_r^2 \tag{27}$$

The flow performance of these two types of regenerators is also evaluated using the Euler number (*Eu*) derived from Eq. (20). Furthermore, the Stanton number (*St*) of the gas in these two types of regenerators can be calculated as:

$$St = \frac{Nu}{Re_h Pr} \tag{28}$$

The regenerator's number of heat transfer units (*NTU*) is determined based on *St* as follows [43]:

$$NTU = \frac{St A_s \varphi}{2 A_r} \tag{29}$$

Therefore, the effectiveness of these two types of regenerators is [44]:

$$\varepsilon_r = \frac{NTU}{NTU + 1} \tag{30}$$

### 3.4. Predication of overall output performance for Stirling engines

In this work, the evaluation of the Stirling engine's overall output performance is conducted based on the actual output power and thermal efficiency. According to the adiabatic model, we can determine the theoretical cyclic heat input and work output as follows [40]:

$$Q_h = \int_{t=0}^{t=\tau} dQ_h \tag{31}$$

$$W_i = \int_{t=0}^{t=\tau} dW_e + \int_{t=0}^{t=\tau} dW_c \tag{32}$$

In Eqs. (31) and (32), $t$ represents time, and $\tau$ denotes the cycle duration of engines.

The cyclic heat loss caused by imperfect regeneration in the Stirling engine is given by [45]:

$$Q_{r,loss} = (1 - \varepsilon_{r,m}) m_g c_{v,f} (T_H - T_K) \tag{33}$$

where $\varepsilon_{r,m}$ denotes the cycle-averaged regenerator effectiveness, $c_{v,f}$ represents the gas's specific heat capacity, and $m_g$ stands for the mass of gas contained within engines.

Hence, the actual heat input rate of the regenerator can be determined as [46]:

$$Q_{ac} = Q_h + Q_{r,loss} \tag{34}$$

$$\dot{Q}_{ac} = Q_{ac} \cdot f \tag{35}$$

The cyclic work loss generated by flow resistance within regenerators is:

$$W_{r,loss} = \int_{t=0}^{t=\tau} |\Delta p_r u_r| A_r \cdot dt \tag{36}$$

Additionally, this work also accounts for the pressure drop losses caused by mechanical resistance and the finite speed of the piston within the engine, with their respective values as follows [45]:

$$\Delta p_f = \frac{(0.4 + 0.0045 Bn) \times 10^5}{3\phi} \left(1 - \frac{1}{r}\right) \tag{37}$$

$$\Delta p_w = \frac{Bn}{60} \left(\frac{4 p_m}{(1 + 1/\zeta)(1 + r)}\right) \left(\frac{r \ln r}{r - 1}\right) \sqrt{\frac{\gamma}{R_g}} \left(\frac{1}{\sqrt{T_K + \Delta T_K}}\right) \left(1 + \sqrt{\frac{T_H - \Delta T_H}{T_K + \Delta T_K}}\right) \tag{38}$$

In Eqs. (37) and (38), $n$ and $p_m$ represent the engine speed and cycle-averaged pressure, $B$ is the piston stroke, $r$ denotes the engine compression ratio, defined as $r = V_{\max}/V_{\min}$, where $V_{\max}$ and $V_{\min}$ represent the peak and valley values of volumes in a cycle, determined from the adiabatic model. $\zeta$ is the temperature ratio, calculated by $\zeta = T_K/T_H$, $\gamma$ signifies the specific heat ratio for the gas, defined as $\gamma = c_{p,f}/c_{v,f}$. $\Delta T_H$ is the temperature difference between the engine's hot end and the heat source, and $\Delta T_K$ stands for the temperature difference between the engine's cold end and the heat sink, both set to 0 in this study. Furthermore, $\phi$ can be expressed as a function of $r$ [45]:

$$\phi = 1 - \frac{1}{3r} \tag{39}$$

The cyclic work losses arising from mechanical pressure drop within the engine and finite piston speed pressure drop are as follows:

$$W_{f,loss} = \Delta p_f (V_{max} - V_{\min}) \tag{40}$$

$$W_{w,loss} = \Delta p_w (V_{\max} - V_{\min}) \tag{41}$$

Consequently, the total energy loss rate, actual output power, and thermal efficiency of the Stirling engine are given by:

$$E_{loss} = (Q_{r,loss} + W_{r,loss} + W_{f,loss} + W_{w,loss}) \cdot f \tag{42}$$

$$P_{ac} = (W_i - W_{r,loss} - W_{f,loss} - W_{w,loss}) \cdot f \tag{43}$$

$$\eta_{ac} = \frac{P_{ac}}{\dot{Q}_{ac}} \tag{44}$$

To obtain quantitative data regarding the engine performance, a study on the overall output performance of engines equipped with different regenerators types is undertaken on the basis of the key specification of the GPU-3 Stirling engine [47]. The primary engine parameters under investigation in this paper are listed in Table 2.

### 3.5. Solution procedure

In this study, we propose a Matlab code to numerically solve the adiabatic model of the Stirling engine using the fourth-order Runge-Kutta method (RK-4). Upon achieving a periodic steady state in the calculations, the ideal output performance of the engine and the boundary conditions of the regenerator are obtained. Subsequently, the variation of the boundary conditions is fitted to transcendental functions and employed as User Defined Functions (UDFs) in the CFD solution of the regenerator model, which is accomplished using the commercial software Fluent. Once the regenerator model calculations converge, the transient values of the physical fields inside the regenerator over the cycle are utilized to determine the variations in the Euler number ($Eu$) and heat transfer effectiveness ($\varepsilon_r$) of the regenerator, and to calculate the pressure drop losses and imperfect regeneration losses of the regenerator. These losses are then incorporated into the ideal output performance of the engine, along with other significant energy losses within the engine, to derive the corrected actual output power and thermal efficiency values of the engine. However, it is noteworthy that correlations for flow and heat transfer characteristics of the other two types of regenerators, namely the Stacked Woven Screen Regenerator (SWSR) and the Parallel Miniature-Channel Regenerator (PMCR), are available in publicly accessible literature. Therefore, for these two types of regenerators, the regenerator boundary conditions obtained from the engine model can be directly used to solve for the $Eu$, $\varepsilon_r$, and various energy loss values using empirical correlations, obviating the need for CFD numerical calculations using Fluent.

## 4. Model verification

### 4.1. Grid independence test

Due to the small size and densely distributed characteristics of the regenerator channels, tetrahedral unstructured grids are adopted to partition both the gas and solid domains. In the gas domain, characterized by intricate flow structures and high temperature gradients, the grid size does not exceed 0.12 mm. Conversely, within the solid domain, where only conduction phenomena occur, a coarser grid size is permissible, with a maximum set at 0.3 mm. The grid size at the gas-solid interface aligns with that of the gas domain.

Furthermore, to mitigate the influence of grid number on numerical outcomes, a grid independence verification is performed, as illustrated in Fig. 2. Three grid systems, consisting of 4.55 million, 9.22 million, and 18.21 million grid elements respectively, are tested to evaluate their impact on the transient variations in pressure drop ($\Delta p_r$) and gas average temperature ($T_{f,ave}$) of the regenerator over a single cycle. It is evident that the transient changes in pressure drop and gas average temperature obtained from the three grid systems exhibit strong agreement. As the grid number escalates from 9.22 million to 18.21 million, the average discrepancies in transient variations for pressure drop and gas average temperature amount to 1.3% and 0.23%, respectively. Hence, it can be inferred that the grid system with 9.22 million grids satisfies the criterion of grid independence. Considering computational accuracy and resource utilization, this study opts for the grid system with 9.22 million grids for computation.

**Table 2**
Key specifications of Stirling engines with different types of regenerators.

| Parameter | Value | Parameter | Value |
|---|---|---|---|
| **General formation** | | Clearance volume | 30.52 cm$^3$ |
| Working gas | Helium | **Heater** | |
| Cylinder diameter | 69.9 mm | Heater temperature | 922 K |
| Piston stroke | 31.2 mm | Dead volume | 70.88 cm$^3$ |
| Phase angle | 90° | **Cooler** | |
| Initial crank angle | 0° | Cooler temperature | 288 K |
| Engine speed | 2500 rpm | Dead volume | 13.8 cm$^3$ |
| Charge pressure | 2.76 MPa | **Regenerator** | |
| **Compression chamber** | | Matrix types | IMCR, SWSR, PMCR |
| Swept volume | 113.14 cm$^3$ | Material | Stainless steel |
| Clearance volume | 28.68 cm$^3$ | Length | 50 mm |
| **Expansion chamber** | | Dead volume | 74.98–139.97 cm$^3$ |
| Swept volume | 120.82 cm$^3$ | Porosity | 0.277–0.517 |

### 4.2. Verification of the reliability for regenerator performance evaluation

To verify the reliability of the mathematical model proposed in this study for characterizing flow and heat transfer characteristics of regenerators, a performance investigation on a heat sink with corrugated plate fins [48] with similar corrugated channel structures and Reynolds number (600–2400) to the inclined-flow miniature-channel regenerator ($Re_h < 1850$) is conducted. Employing the same numerical methods, we compare the computed results with experimental data for flow and heat transfer performance under identical operating conditions. The geometry and primary parameters of the heat sink with corrugated plate fins are detailed in Fig. 3 and Table 3, respectively.

Fig. 4 presents a comparative overview of numerical results and experimental data. The uncertainty of pressure drop and gas-solid convective heat transfer coefficient ($h = q/(T_{w,m}\text{-}T_{f,m})$, where $q$, $T_{w,m}$, and $T_{f,m}$ are the heat flux, average surface temperature of the heat sink, and average gas temperature, respectively) is only ±0.5% and ± 2.98%, respectively, indicating high reliability of the experimental findings. The analysis reveals a close agreement between the pressure drop and the convective heat transfer coefficient of the heat sink obtained through numerical simulations and experimental measurements. The average deviations between the two methods for pressure drop and heat transfer coefficient are 10.5% and 6.5%, respectively. The maximum deviation of 26% occurs in the pressure drop at a $Re$ of 600, where the

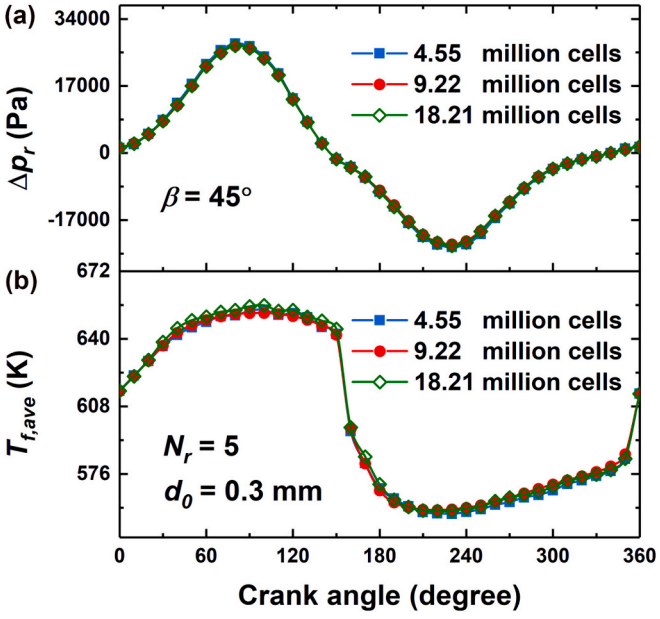


**Fig. 2.** Transient variations in pressure drop and gas average temperature of the regenerator over a single cycle under three grid systems with different grid numbers.

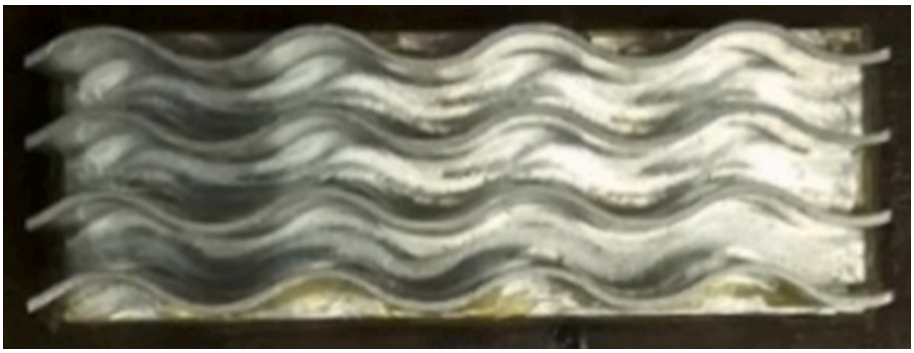

**Fig. 3.** Geometries of the heat sink with corrugated plate fins.

**Table 3**
Specifications of the heat sink with corrugated plate fins.

| Parameter | Value |
|---|---|
| Amplitude | 2 mm |
| Wavelength | 18.68 mm |
| Total length | 75 mm |
| Height | 25 mm |
| Width | 6 mm |
| Thickness | 1 mm |
| Inlet temperature | 287.3 K |

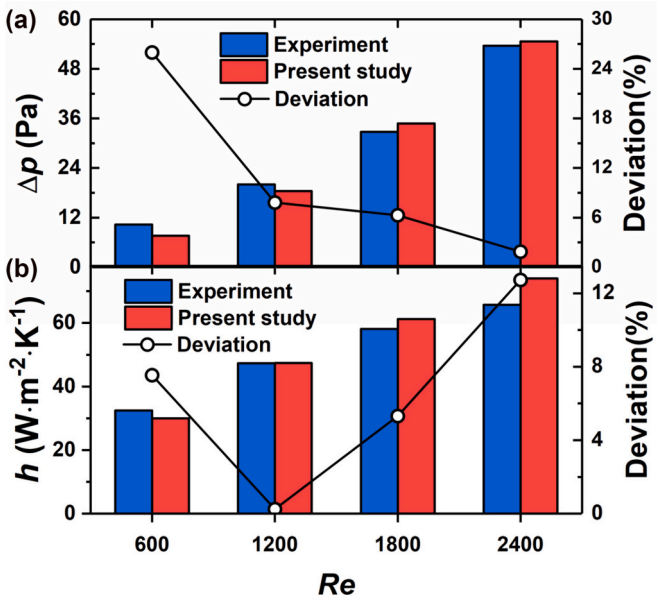


**Fig. 4.** Comparison of numerical results and experimental data for the corrugated plate-fin heat sink.

experimental pressure drop value is only 10.3 Pa. In reality, each pressure gauge in the experiment has a certain level of uncertainty, and measuring such a small pressure drop itself may introduce relatively high test errors. Therefore, the 26% relative deviation associated with the calculated pressure drop of 7.6 Pa in this study is considered acceptable. These results indicate that the mathematical model proposed in this study exhibits relatively robust predictive capabilities for the flow and heat transfer patterns within corrugated channels and can be effectively employed to evaluate the thermal and flow performance of inclined-flow miniature-channel regenerators.

### *4.3. Verification of the accuracy for Stirling engine performance predication*

On the other hand, to verify the accuracy of the predictive approach for the engine's overall output performance outlined in Section 3.4, this study applies the method to derive the comprehensive output performance of the GPU-3 Stirling engine and compares it with corresponding experimental data [47]. The key specifications for the GPU-3 Stirling engine in tests of the literature are summarized in Table 4. Fig. 5 offers a visual representation of the comparison between the predicted actual output power and thermal efficiency values and those obtained from experimental tests at different average pressure ($p_m$). The results demonstrate a maximum deviation of 23.2% and an average deviation of 10.7% between the calculated output power and test results across three different average pressures. Similarly, the maximum and average deviation between the predicted thermal efficiency value and experimental data are 5.5% and 4.6%, respectively. These results illustrate a relatively high level of consistency between the predictions and experimental data, underscoring the considerable accuracy of the engine performance prediction method proposed in this paper.

## 5. Results and discussion

### *5.1. Thermal and flow characteristics in regenerators*

#### *5.1.1. Distribution of localized characteristics*

To explore the impact of corrugated inclined miniature-channel structures within the regenerator on internal gas flow and heat transfer patterns, as well as to comprehend the underlying mechanisms behind the overall performance enhancement of novel inclined-flow miniature-channel regenerators, this study commences by analyzing the distribution of localized thermal and flow characteristics within regenerators.

Fig. 6 illustrates the physical field profiles within the inclined-flow

**Table 4**
Specifications of the GPU-3 Stirling engines from literature experiments.

| Parameter | Value | Parameter | Value |
|---|---|---|---|
| **General information** | | **Heater** | |
| Working gas | Helium | Heater temperature | 922 K |
| Cylinder diameter | 69.9 mm | Dead volume | 70.88 $cm^3$ |
| Piston stroke | 31.2 mm | **Cooler** | |
| Engine speed | 2500 rpm | Cooler temperature | 286 K |
| Charge pressure | 2.76–5.52 MPa | Dead volume | 13.8 $cm^3$ |
| Phase angle | 90° | **Regenerator** | |
| **Compression chamber** | | Matrix type | Woven screen |
| Swept volume | 113.14 $cm^3$ | Material | Stainless steel |
| Clearance volume | 28.68 $cm^3$ | Length | 22.6 mm |
| **Expansion chamber** | | Dead volume | 50.55 $cm^3$ |
| Swept volume | 120.82 $cm^3$ | Wire diameter | 0.04 mm |
| Clearance volume | 30.52 $cm^3$ | Porosity | 0.697 |

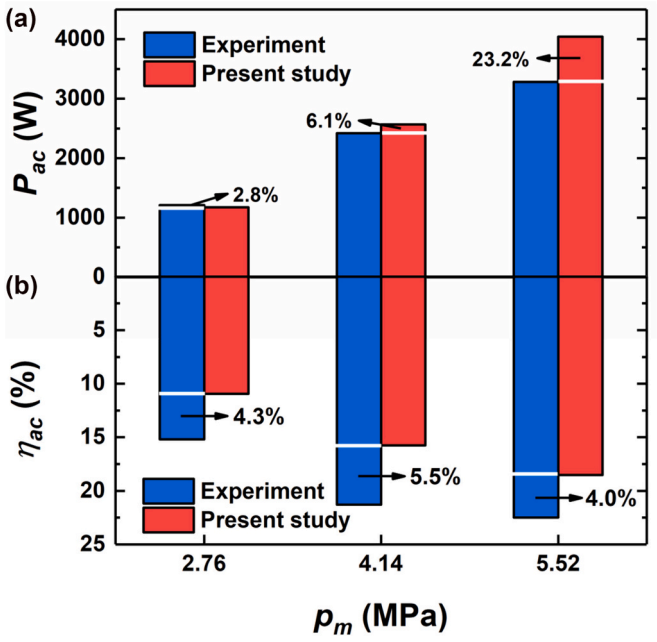


**Fig. 5.** Comparison between the predicted actual output power and thermal efficiency values and those obtained from experimental tests.

miniature-channel regenerator when the average gas velocity reaches its maximum during the hot blow phase. Here, vorticity magnitude ($w$) is defined as the curl of the gas velocity vector, representing the intensity of swirling motion within the gas flow. Observations reveal that as the gas periodically traverses the peaks or valleys of the corrugated channel, the substantial alteration in flow direction due to centrifugal forces not only directs the gas to sweep across the opposite matrix surface at specific inclined angles (marked by red dashed box in Fig. 6 (a-1)) but also induces vigorous local turbulence and swirling flows near the steering point (evidenced by a significant increase in vorticity magnitude in Fig. 6 (b-1)). This phenomenon accelerates the gas's cross-layer mixing, thereby reducing the thermal boundary layer thickness within the channel and amplifying the gas's temperature gradient near the matrix surface (marked by blue dashed box in Fig. 6 (a-2)). Consequently, gas-solid heat transfer performance is significantly enhanced, resulting in greater variations in gas temperature and an increase in the temperature difference between the cold and hot ends of the regenerator. On the contrary, the robust interaction between the gas and the matrix at the peaks and valleys leads to a pronounced drop in pressure potential energy.

However, as the gas gradually moves away from the steering point, the disturbance intensity of the gas on the channel surface diminishes rapidly (indicated by a significant reduction in vorticity magnitude). Simultaneously, the gas's flow direction gradually aligns with the extended direction of the channel surface, weakening the inclined flush on the heat transfer surface. Consequently, the local heat transfer performance of the regenerator weakens compared to that at the peaks and valleys, and the rate of temperature decrease of the gas lessens. Additionally, the kinetic energy associated with sustaining local turbulence and swirling motion in the gas is partially regained and converted into pressure potential energy. This leads to a local pressure increase in the gas after overcoming resistance losses along the path. In conclusion, owing to the near absence of flow separation phenomena and flow stagnation regions within the regularly structured matrix, the gas pressure drop within the inclined-flow miniature-channel regenerator remains relatively low. Turbulence and local swirling flow phenomena induced by changes in gas flow direction at the peak and valley seem to be the main sources of pressure losses within this regenerator.

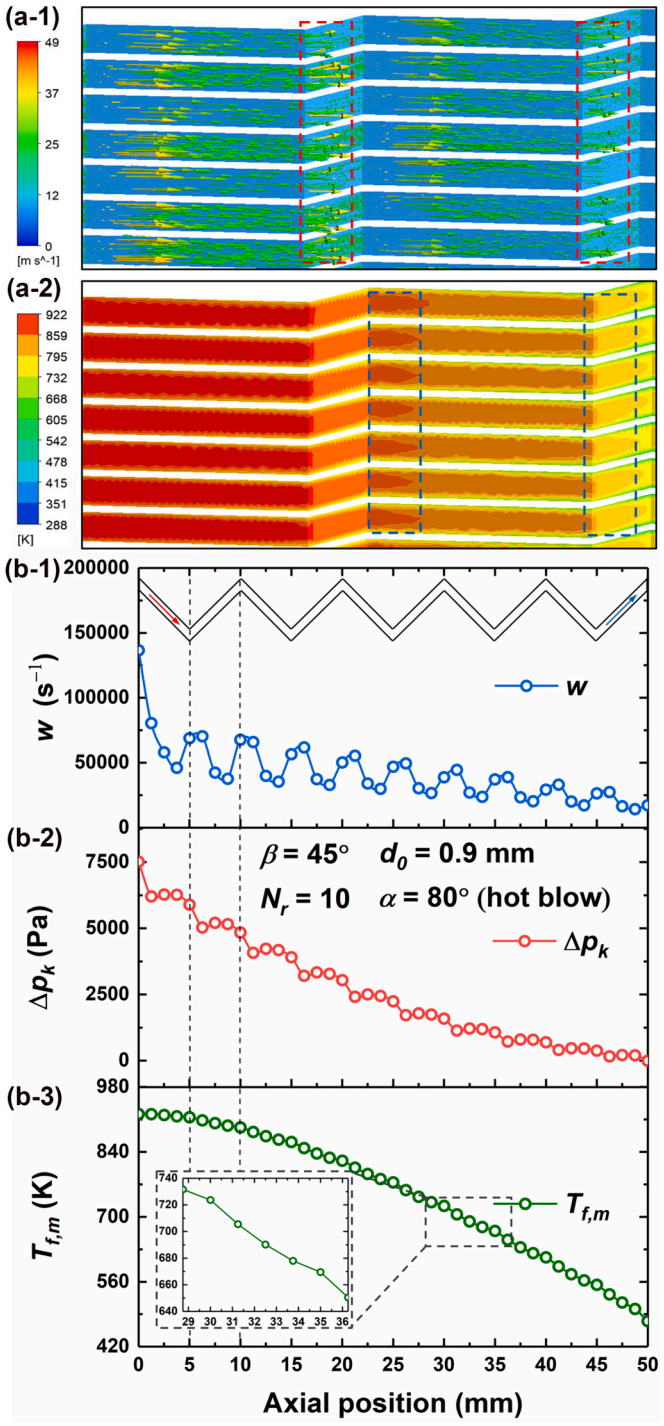


**Fig. 6.** Physical field profiles of gas in the inclined-flow miniature-channel regenerator: (a) local velocity vector and temperature contour and (b) axial profiles of vorticity magnitude, pressure difference relative to the cold end, and temperature.

### 5.1.2. *Periodic variation of transient characteristics*

Within the engine, the regenerators operate under complex oscillating flow conditions, and how its thermal and flow characteristics respond to changing boundary conditions directly impacts the regenerator's cycle-averaged performance. Therefore, an in-depth analysis of the transient thermal and flow characteristics within inclined-flow miniature-channel regenerators is conducted.

Fig. 7 provides insight into the fluctuations in transient gas flow performance within the regenerator over a single cycle. The average

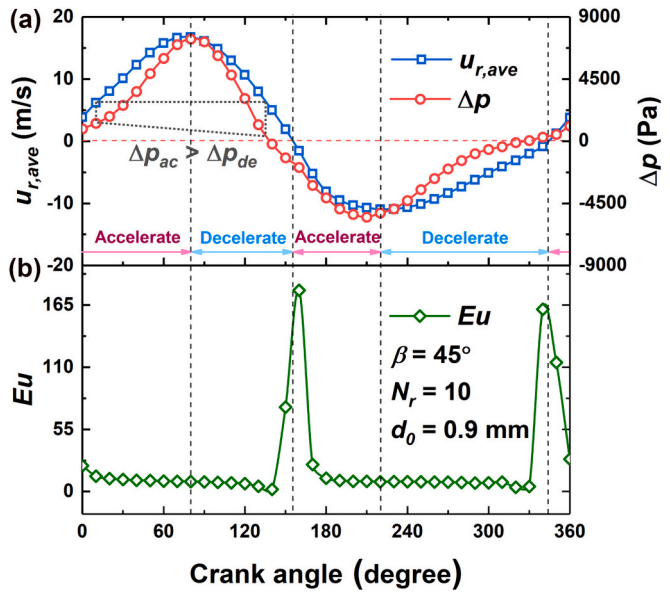


**Fig. 7.** Variations in transient gas flow performance in the regenerator over a single cycle.

velocity of the regenerator ($u_{r,ave}$) serves to characterize the overall gas flow direction within it. A positive $u_{r,ave}$ denotes gas flow from the hot end to the cold end, while a negative $u_{r,ave}$ indicates gas flow from the cold end back to the hot end. Similarly, the sign of $\Delta p$ signifies the direction of pressure drop within the regenerator, with $\Delta p > 0$ indicating pressure reduction from the hot end toward the cold end and *vice versa*. It can be observed that gas velocity experiences alternating phases of acceleration and deceleration in both the positive and negative flow directions during the cycle, resulting in an overall variation pattern closely approximating a sinusoidal function. When gas flows from the cold end, driven by its lower temperature and thus higher density, its velocity peak is relatively smaller. The overall variation in gas pressure drop within the regenerator broadly mirrors the velocity fluctuations.

However, in contrast to the monotonic pressure drop changes with velocity seen in steady flows, oscillating flows often exhibit higher gas pressure drops during acceleration phases compared to deceleration phases. This phenomenon stems from the fact that pressure drop in oscillatory flows primarily results from two key factors: resistance losses due to gas flow along the path and the consumption of pressure potential energy caused by local acceleration effects. During acceleration phases, where the direction of gas velocity aligns with that of local acceleration, the total pressure drop equals the linear summation of the pressure drops resulting from these two factors. Conversely, during the deceleration phase, when the gas experiences local acceleration in the opposite direction to the flow, it partly counteracts the pressure drop incurred by gas flow along the path, leading to a reduction in the total pressure drop. As gas velocity decreases, the local acceleration effect progressively intensifies, hence this phenomenon will become more pronounced. Especially near the velocity reversal moment, very low gas velocity results in a pressure drop along the path lower than the pressure drop induced by local acceleration in the opposite direction, creating a unique scenario where the velocity direction opposes the total pressure drop direction.

The Euler number (*Eu*), which remains independent of gas velocity magnitude, can distinctly manifest the local acceleration effect of the gas. In the vicinity of the velocity reversal moment, gas acceleration peaks while gas velocity bottoms out. At this time, the local acceleration effect becomes significant, thus resulting in a substantial increase in *Eu*. During acceleration phases, with the increase of gas velocity, the local acceleration effect weakens, which brings about a reduction in *Eu*. Conversely, during the deceleration phase, as gas velocity starts to decrease while the local acceleration effect in the opposite direction gradually intensifies, *Eu* continues to diminish until gas velocity reverses its direction.

Fig. 8 elucidates the variations in the transient heat transfer performance for inclined-flow miniature-channel regenerators throughout a single cycle. When the crank angle spans from −10 to 150°, gas inflow occurs at the regenerator's hot end, featuring an average temperature surpassing that of the matrix. Consequently, heat transfers from the gas to the matrix, initiating a gradual uptick in matrix temperature. This phase is referred to as the hot blow phase. Transitioning to the range of 150 to 350 degrees of crank angles, gas enters from the cold end, with its average temperature falling below that of the matrix. Herein, the matrix begins to emit heat to the gas, resulting in a gradual decline in matrix temperature. This phase is known as the cold blow phase.

In each phase, the heat transfer between the gas and the matrix is influenced by residual gas from the preceding phase. Consider the hot blow phase, where the onset of hot gas flow into the regenerator's hot end expels the previously trapped cold gas from the prior cold blow phase, forcing it out through the cold end. Consequently, the average temperature of the gas gradually increases. As the gas traverses the entire regenerator, the expulsion of the remaining cold gas from the previous phase is complete, concurrently with the gas velocity oscillations entering the deceleration phase. As gas velocity decreases, the duration of heat transfer between the gas and the matrix becomes more extensive, resulting in a gradual decline in gas temperature. The temperature variation mechanism during the cold blow phase mirrors this process, but with reversed tendencies due to the alteration in gas-solid heat transfer direction. In each phase, as the temperature difference between the gas and the matrix initially increases and then decreases, the regenerator heat loss caused by gas-solid heat transfer with a finite temperature difference follows a similar trend, thus leading to a variation of initially decreasing and then increasing for the regenerator effectiveness.

### 5.2. Sensitivity analysis of regenerator and Stirling engine performance

In the subsequent analysis, we delve into the impact of primary geometric variables of the inclined-flow miniature-channel regenerator on thermal and flow characteristics of regenerators, as well as the

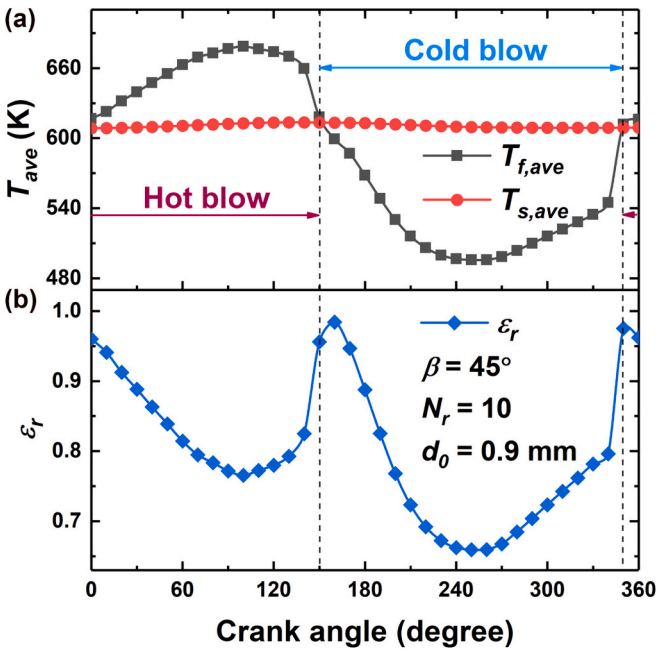


**Fig. 8.** Variations in the transient flow performance for the inclined-flow miniature-channel regenerator over a single cycle.

overall output performance of engines. Fig. 9 displays the Euler number ($Eu$) and effectiveness ($\varepsilon_r$) of the regenerator, and total energy loss ($E_{loss}$) of the engine, all across various inclined angles ($\beta$) applied to the matrix miniature channels. As one of the most crucial structural parameters for the inclined-flow regenerator, the inclined angle of the miniature channel significantly impacts the flow and heat transfer performance of the regenerator. With an increasing inclined angle, the guiding effect of the matrix surface at the peaks and valleys in the corrugated channels on the gas steering is enhanced, leading to a heightened centrifugal force experienced by the gas as it passes through these regions. This not only enhances the gas's ability to flush the matrix surface behind the steering regions but also amplifies turbulence and swirling flows near the peaks and valleys, consequently increasing pressure losses of regenerators.

Moreover, under the constant axial length of the regenerator, an increased inclined angle implies a longer actual flow path for the gas within the regenerator. This causes higher resistance losses along the flow path, further accentuating the regenerator's flow characteristics. However, the increase in the inclined angle not only enlarges the overall gas-solid heat transfer area within the regenerator but also augments the interaction between the gas and the matrix surface. This results in an accelerated cross-layer mixing of the gas and improved temperature uniformity within the core flow region of the channels, ultimately bringing about a substantial enhancement in the regenerator's thermal performance.

It's worth noting that while structural parameters of the regenerator change, non-regenerator losses, such as engine mechanical friction and finite piston speed losses, show relatively minor variations. Consequently, the effect of geometric parameters on the comprehensive thermal and flow performance of regenerators can be effectively captured through changes in the engine's total energy loss ($E_{loss}$), as depicted in Fig. 9 (c). It is evident that, across different inclined angles, despite the significant amplitude of opposite changes in flow and heat transfer performance of the inclined-flow miniature-channel regenerator, the proportion of pressure drop losses remains relatively low due to the regenerator's inherently low base value of flow resistance. Instead, the primary contributor to the regenerator's total energy loss is heat loss resulting from imperfect regeneration. As a result, as the inclined angle increases, regenerator effectiveness improves, and the overall performance of the regenerator enhances due to the reduction in losses attributed to imperfect regeneration.

Fig. 10 presents the variations in overall output performance of the Stirling engine at different inclined angles ($\beta$) applied to the matrix miniature channels. Despite the fact that pressure losses within the regenerator constitute a relatively modest proportion of the total energy losses, these losses directly deplete the pressure potential energy of the gas within the engine's working chambers, which is essential for driving the piston and performing work. Consequently, with the increasing inclined angle, there is a non-negligible reduction in the engine's actual output power ($P_{ac}$) due to the increasing pressure drop losses. However, with an elevation in the inclined angle, the simultaneous rise in regenerator substantially diminishes the imperfect regeneration losses within the regenerator, consequently bringing about a marked reduction in the total heat absorption demanded by engines, so that the thermal efficiency ($\eta_{ac}$) of engines is increased instead.

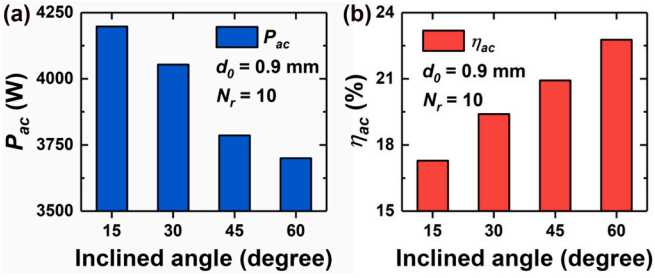


**Fig. 10.** Output power and thermal efficiency of engines at different inclined angles applied to the matrix miniature channels.

The opposing trend observed in the output power and thermal efficiency of Stirling engines with the increasing inclined angle suggests the presence of an optimal angle for the matrix channel within the investigated range of 15 to 60°, where the comprehensive output performance of engines is maximized. This discovery contradicts the consistent improvement seen in the overall thermal and flow performance of the regenerator with increasing inclined angle. It underscores that relying solely on component-based analysis of regenerator characteristics is insufficient for evaluating the application potential of regenerators, and thereby demonstrating the significance to investigate the effect of regenerators on engine performance at the system level in this paper.

As depicted in Fig. 10, it is apparent that within the inclined angle range of 30 to 45°, the inclined-flow miniature-channel regenerator attains relatively harmonious balance between output power and thermal efficiency. Consequently, in subsequent geometric designs, we have opted to maintain the inclined angle ($\beta$) of the regenerator matrix channels at a fixed 45°. Fig. 11 provides an overview of the comprehensive performance variations exhibited by the inclined-flow miniature-channel regenerator across different sub-regenerator numbers ($N_r$) and channel diameters ($d_0$). It is discernible that notable shifts occur in the regenerator's mass and heat transfer performance within the ranges of 5 to 15 sub-regenerators and 0.3 to 1.5 mm channel diameters. As the number of sub-regenerators increases, the pitch between the peaks and valleys of the corrugated channels within the regenerator diminishes. This results in a more frequent direction alteration of the gas flow, leading to intensified local turbulence and swirling flow phenomena. This heightened intensity of gas-solid interactions, in turn, leads to a decline in flow performance while concurrently enhancing heat transfer performance within the regenerator. Additionally, the increased frequency of changes in flow direction expands the area where the gas interacts with the matrix surface near the steering regions, further amplifying the heat exchange rate between the gas and the matrix. Ultimately, this contributes to an improvement in regenerator effectiveness.

Maintaining a constant number of sub-regenerators, an increase in channel diameter results in a larger effective flow area within the

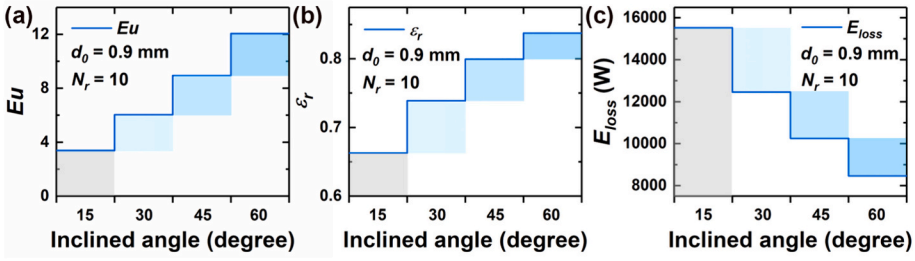


**Fig. 9.** Euler number and effectiveness of the regenerator, and total energy loss of the engine, all across various inclined angles applied to the matrix miniature channels.

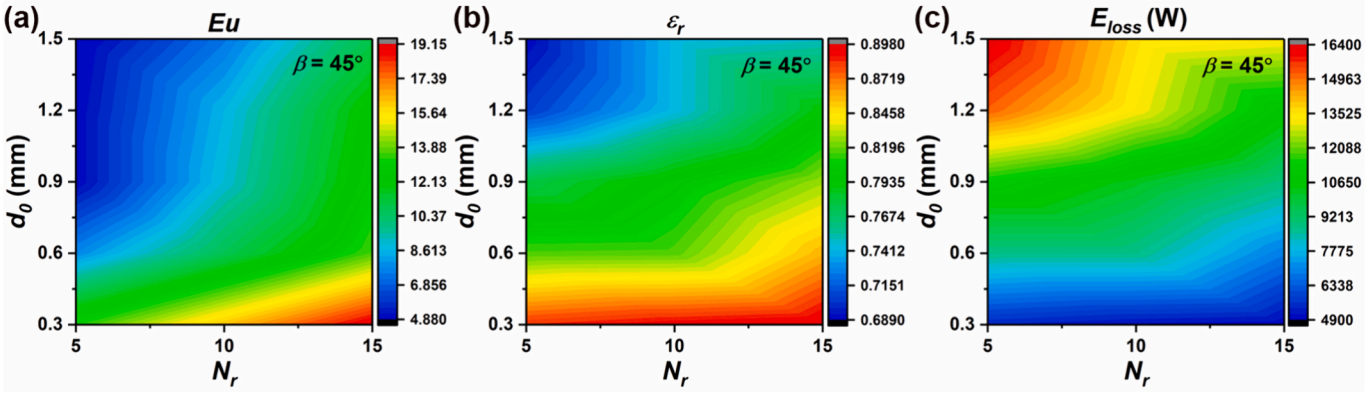


**Fig. 11.** Performance variations exhibited by the inclined-flow miniature-channel regenerator across different sub-regenerator numbers and channel diameters.

regenerator. This, in turn, lowers the average gas velocity within the channels, subsequently reducing turbulence and swirling flow intensity. Consequently, both pressure losses and gas-solid heat exchange rates within the regenerator concurrently decrease. Furthermore, an increase in flow channel diameter diminishes the velocity and temperature gradients of the gas along the radial direction of the channels within the regenerator. This reduction, in turn, lessens the viscous shear stress between different flow layers within the gas, and diminishes both gas cross-layer heat transfer and gas-solid convective heat exchange. This further results in an overall improvement in flow performance but a reduction in heat transfer performance within regenerators. However, as elucidated in Fig. 11 (c), owing to imperfect regeneration losses predominantly governing the total losses of regenerators, the response trend of the comprehensive thermal and flow performance of the regenerator to these two geometric parameters closely mirrors that of the regenerator effectiveness. In other words, they increase with an augmentation in the number of sub-regenerators and a reduction in channel diameter.

The variation in the overall output performance of Stirling engines under different sub-regenerator numbers and channel diameters is depicted in Fig. 12. As depicted in Fig. 12 (a), the pressure drop losses in the inclined-flow miniature-channel regenerator exhibits a relatively low base value, thereby imparting a limited influence on the engine's output power, which ranges from 3616 to 4214 W. However, Fig. 12 (b) illustrates that substantial variations in regenerator effectiveness lead to notable discrepancies in the actual heat absorption by the engine. This, in turn, causes a significant alteration in the engine's thermal efficiency, ranging from 15.3% to 29.7%. In Fig. 12 (c), an increase in the sub-regenerators number results in diminished regenerator flow performance, leading to increased pressure drop losses within regenerators and a slight reduction in the engine's actual output power. Nevertheless, the simultaneous improvement in regenerator effectiveness significantly mitigates imperfect regeneration losses, resulting in a more substantial decrease in the engine's actual heat absorption compared to the output power. Consequently, there is an increase in the engine's thermal efficiency.

In contrast to the sub-regenerator number, the impact of changes in regenerator channel diameter on Stirling engine performance is relatively intricate, as shown in Fig. 12 (d). With an increase in channel diameter, the reduced gas flow velocity within the regenerator and

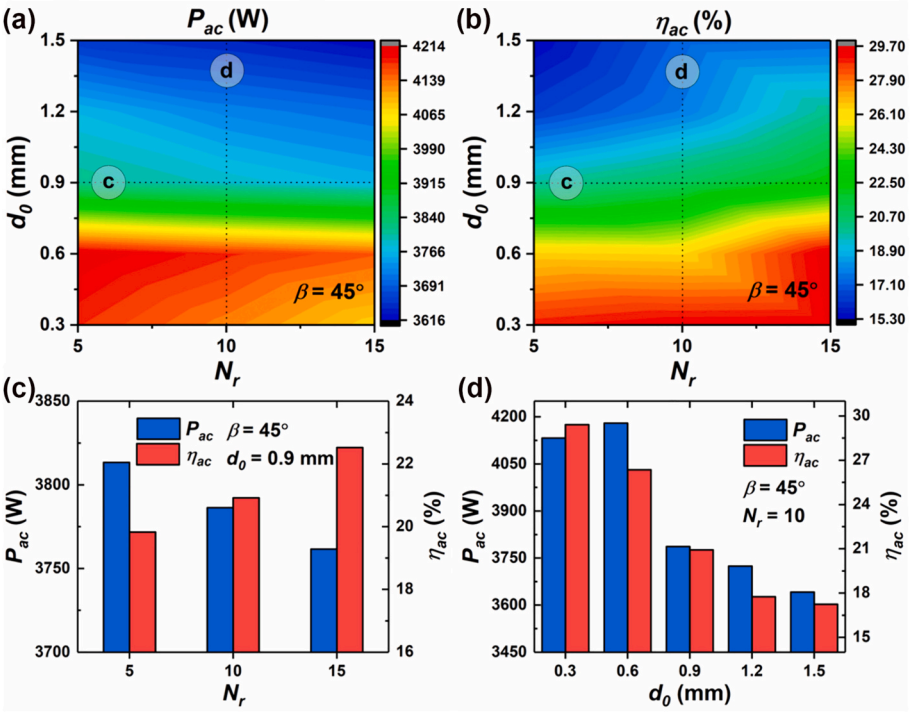


**Fig. 12.** Variations in the overall output performance of engines under different sub-regenerator numbers and channel diameters.

diminished shear stress between different flow layers reduce the power losses attributed to pressure drop within the regenerator. Consequently, the engine's actual output power increases. Whereas, the increase in channel diameter also enlarges the dead volume within the regenerator, resulting in a substantial decrease in the average gas pressure within the engine. This substantially diminishes the engine's ability to perform work *via* the piston, leading to an evident reduction of the engine's ideal output power. Under the combined influence of these two opposing mechanisms, the engine's actual output power demonstrates an initial increase followed by a decrease trend with increasing channel diameter, reaching its maximum at a channel diameter of approximately 0.6 mm. Moreover, the weakened heat transfer performance of the regenerator increases the heat absorption demand of the engine, consequently resulting in remarkably reduction in the engine's thermal efficiency. Based on the aforementioned analysis, for achieving higher overall engine performance, it is recommended, when designing the inclined-flow miniature-channel regenerators, to opt for a larger number of sub-regenerators and a smaller channel diameter.

### 5.3. Comparative performance analysis for different types of regenerators

In this section, the thermal and flow performance of inclined-flow miniature-channel regenerators (IMCR), as well as the engine's overall output performance when equipped with this regenerator, are compared with those of the commonly used cross-flow and parallel-flow regenerators, represented by stacked woven screen regenerators (SWSR) and parallel miniature-channel regenerators (PMCR), respectively. This comparative analysis aims to validate the potential application of the IMCR in Stirling engines.

Fig. 13 presents the regenerator's Euler number (*Eu*) and effectiveness ($\varepsilon_r$), along with the energy distributions of Stirling engines, for the SWSR, PMCR, and two IMCR geometries with two extreme values of engine thermal efficiency (min: minimal, max: maximum). Notably, the *Eu* and $\varepsilon_r$ of the IMCR fall within the range of the SWSR and PMCR, indicating that IMCR achieves the intended thermal and flow characteristics as designed for inclined-flow regenerators. The comparison of the engine's overall output performance indicates that despite SWSR significantly mitigates imperfect regeneration losses ($\dot{Q}_{r,loss}/\dot{Q}_{ac} = 4.1\%$) due to its superior regenerator effectiveness, it exhibits comparatively lower flow performance. Consequently, the power loss ($P_{loss}/\dot{Q}_{ac} = 35.5\%$) in the engine caused by regenerator pressure drop is substantial, leading to significantly lower actual output power ($P_{ac} = 0.97$ kW) compared to other types of regenerators, with the thermal efficiency ($\eta_{ac} = 13.1\%$) moderately positioned among the three regenerators. In addition, PMCR exhibits the lowest flow resistance, leading to low power losses ($P_{loss}/\dot{Q}_{ac} = 0.5\%$) within the engine, thus achieving the highest actual output power ($P_{ac} = 4.02$ kW). However, caused by its lower heat transfer performance, significant heat losses ($\dot{Q}_{r,loss}/\dot{Q}_{ac} = 76.7\%$) during the regeneration process increase the engine's demand for heat absorption, ultimately resulting in lower thermal efficiency ($\eta_{ac} = 11\%$) than the other two types of regenerators.

In summary, compared to SWSR and PMCR, engines equipped with IMCR experience a significant reduction in imperfect regeneration and power losses, achieving a well-balanced energy distribution within the engine and higher overall performance. After structural improvement (as illustrated in Fig. 13 (b-4)), IMCR demonstrates a remarkable 325% increase in output power and a 127% increase in thermal efficiency than SWSR. In comparison to PMCR, it achieves a 3% increase in output power and a 171% increase in thermal efficiency. This validates the viability for the design concept of inclined-flow regenerators and the corresponding construction of inclined-flow miniature-channel regenerators in improving the engine's overall output performance.

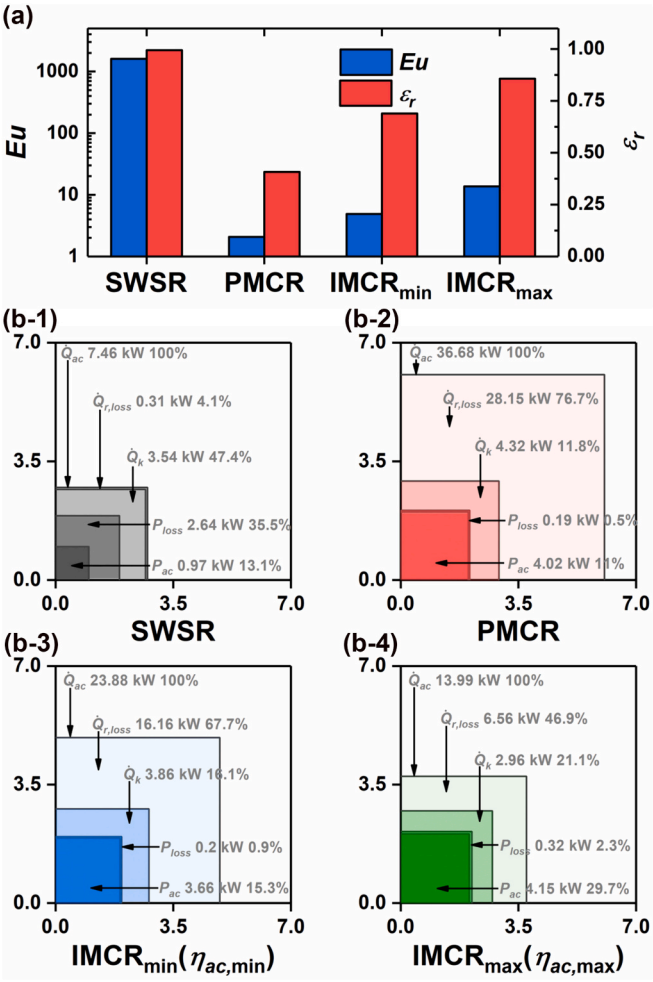


**Fig. 13.** Comparison of regenerator's thermal and flow characteristics, as well as engine's overall output performance under different types of regenerators.

## 6. Conclusions

This work introduced an innovative design concept of inclined-flow regenerators, with the matrix surface inclined to the gas flow direction. Subsequently, an inclined-flow miniature-channel regenerator was constructed based on this concept with the aim of improving the overall performance of Stirling engines. The response mechanisms of the regenerator's thermal and flow characteristics under complex oscillating flow conditions were analyzed, and the comprehensive performance of both the regenerator and the engine under different matrix geometric parameters was studied and compared with that of cross-flow and parallel-flow regenerators. Several noteworthy findings have emerged from this research:

1. Within the corrugated flow channels of the regenerator, the gas undergoes velocity steering at the peaks and valleys. This phenomenon not only directs the gas to effectively sweep across the matrix surface but also induces turbulence and swirling flows in the vicinity of these regions. These effects expedite the movement and cross-layer mixing of the gas. Consequently, the temperature uniformity of the gas in the regenerator becomes excellent, resulting in more pronounced temperature gradients and heightened heat transfer performance in regenerators. Simultaneously, this regenerator exhibits minimal separation phenomena and flow stagnation zones. In this context, the turbulence and swirling flows at peaks and valleys emerge as the predominant sources of flow resistance within the regenerator. As a result, pressure drop within the regenerator experiences significant

suppression.

2. The gas experiences alternate acceleration and deceleration, generating a local acceleration effect that contributes to additional flow pressure drop. This, in conjunction with flow resistance along the path, collectively dictates the regenerator's instantaneous total pressure drop losses. Specifically, during the deceleration process, frictional resistance along the flow path is partly offset by pressure variations from the reverse local acceleration, resulting in lower total pressure drop compared to the acceleration phase at the same velocity. Moreover, the alternation between gas acceleration and deceleration, combined with changes in flow direction, causes periodic temperature oscillations in the gas and matrix during hot and cold blow phases. In each phase, the temperature difference between gas and solid and associated regeneration losses initially rise and then decline.

3. As the channel inclined angle and the number of sub-regenerators increase, the overall intensity of turbulence and swirling flows within the regenerator intensifies. This leads to a decline in the regenerator's flow performance and an increase in power losses, resulting in reduced engine output power. However, these enhanced flow phenomena also facilitate gas's cross-layer movement and mixing, reducing the temperature boundary layer thickness near the matrix surface. This enhances gas-solid heat exchange, significantly elevating the regenerator effectiveness. Consequently, imperfect regeneration losses in the engine decrease significantly, leading to improved thermal efficiency. Furthermore, with an increase in channel diameter, the intensity of turbulence and swirling flows at velocity steering regions decrease, and gas-solid interactions weaken. Additionally, velocity and temperature gradients within the channels decrease significantly. These effects reduce pressure losses but increase heat transfer losses within the regenerator. However, the larger dead volume resulted from the increased channel diameter significantly reduces the engine's ideal output power. As a result, the actual output power initially increases slightly but then exhibits an overall decrease. This, along with an increased demand for heat absorption, results in a decrease in thermal efficiency.

4. In contrast to cross-flow and parallel-flow regenerators, inclined-flow miniature-channel regenerators successfully attains the desired balance in thermal and flow characteristics, aligning with the construction objectives of inclined-flow regenerators. When equipped with this regenerator, the engine effectively mitigates the power losses due to pressure drop and the imperfect regeneration losses arising from heat transfer with finite temperature differences, thus achieving higher overall output performance. As a result, the design concept of the inclined-flow regenerators and the inclined-flow miniature-channel regenerators constructed on the basis of this concept can be preliminarily regarded as holding significant potential to enhance the comprehensive performance of Stirling engines. In forthcoming research, more efficient geometries across a broader spectrum of operational parameters will be explored to further substantiating the feasibility of such inclined-flow regenerators.

## CRediT authorship contribution statement

**Minjie Yu:** Writing – review & editing, Writing – original draft, Visualization, Validation, Software, Methodology, Investigation, Formal analysis, Data curation, Conceptualization. **Lei Xu:** Writing – review & editing, Software, Methodology. **Haichuan Cui:** Writing – review & editing, Software, Methodology. **Zhichun Liu:** Writing – review & editing, Supervision, Resources, Project administration, Funding acquisition. **Wei Liu:** Writing – review & editing, Supervision, Resources, Project administration, Funding acquisition, Conceptualization.

## Declaration of competing interest

The authors do not have any possible conflicts of interest.

## Data availability

Data will be made available on request.

## Acknowledgements

This work was supported by the National Natural Science Foundation of China (Grant No. 51736004).

## References

[1] A. Shrestha, A.A. Mustafa, M.M. Htike, V. You, M. Kakinaka, Evolution of energy mix in emerging countries: modern renewable energy, traditional renewable energy, and non-renewable energy, Renew. Energy 199 (2022) 419–432.
[2] K. Khan, C.W. Su, A. Khurshid, M. Qin, Does energy security improve renewable energy? A geopolitical perspective, Energy 282 (2023) 128824.
[3] S. Zare, A.R. Tavakolpour-Saleh, Modeling, construction, and testing of a diaphragm thermoacoustic Stirling engine, Energy Convers. Manag. 243 (2021) 114394.
[4] H. Hachem, R. Gheith, F. Aloui, S. Ben Nasrallah, Technological challenges and optimization efforts of the Stirling machine: a review, Energy Convers. Manag. 171 (2018) 1365–1387.
[5] M.H. Ahmadi, H. Hosseinzade, H. Sayyaadi, A.H. Mohammadi, F. Kimiaghalam, Application of the multi-objective optimization method for designing a powered Stirling heat engine: design with maximized power, thermal efficiency and minimized pressure loss, Renew. Energy 60 (2013) 313–322.
[6] S. Zhu, G. Yu, K. Liang, W. Dai, E. Luo, A review of Stirling-engine-based combined heat and power technology, Appl. Energy 294 (2021) 116965.
[7] Z. Luo, U. Sultan, M. Ni, H. Peng, B. Shi, G. Xiao, Multi-objective optimization for GPU3 Stirling engine by combining multi-objective algorithms, Renew. Energy 94 (2016) 114–125.
[8] M. Babaelahi, H. Sayyaadi, Modified PSVL: a second order model for thermal simulation of Stirling engines based on convective–polytropic heat transfer of working spaces, Appl. Therm. Eng. 85 (2015) 340–355.
[9] M. Babaelahi, H. Sayyaadi, A new thermal model based on polytropic numerical simulation of Stirling engines, Appl. Energy 141 (2015) 143–159.
[10] S. Alfarawi, R. Al-Dadah, S. Mahmoud, Influence of phase angle and dead volume on gamma-type Stirling engine power using CFD simulation, Energy Convers. Manag. 124 (2016) 130–140.
[11] A.S. Nielsen, B.T. York, B.D. MacDonald, Stirling engine regenerators: how to attain over 95% regenerator effectiveness with sub-regenerators and thermal mass ratios, Appl. Energy 253 (2019) 113557.
[12] P.V. Trevizoli, J.R. Barbosa, Entropy generation minimization analysis of oscillating-flow regenerators, Int. J. Heat Mass Transf. 87 (2015) 347–358.
[13] M. Liu, B. Zhang, D. Han, X. Du, H. Wang, Experimental study on regenerative effectiveness and flow characteristics of parallel-plate regenerator in Stirling engine, Appl. Therm. Eng. 217 (2022) 119139.
[14] M. Tanaka, I. Yamashita, F. Chisaka, Flow and heat transfer characteristics of the Stirling engine regenerator in an oscillating flow, JSME Int. J. 33 (2) (1990) 283–289.
[15] K. Yanaga, R. Li, S. Qiu, Robust foil regenerator flow loss and heat transfer tests under oscillating flow condition, Appl. Therm. Eng. 178 (2020) 115525.
[16] R. Gheith, F. Aloui, S. Ben Nasrallah, Determination of adequate regenerator for a Gamma-type Stirling engine, Appl. Energy 139 (2015) 272–280.
[17] Y. Kato, K. Baba, Empirical estimation of regenerator efficiency for a low temperature differential Stirling engine, Renew. Energy 62 (2014) 285–292.
[18] S. Alfarawi, R. Al-Dadah, S. Mahmoud, Transient investigation of mini-channel regenerative heat exchangers: combined experimental and CFD approach, Appl. Therm. Eng. 125 (2017) 346–358.
[19] S.K. Garg, B. Premachandran, M. Singh, S. Sachdev, M. Sadana, Effect of porosity of the regenerator on the performance of a miniature Stirling cryocooler, Thermal Sci. Eng.Progr. 15 (2020) 100442.
[20] M. Yu, C. Shi, J. Xie, P. Liu, Z. Liu, W. Liu, Constructal design of a circular micro-channel Stirling regenerator based on exergy destruction minimization, Int. J. Heat Mass Transf. 183 (2022) 122240.
[21] C. Yu, D. Shen, W. He, Z. Hu, S. Zhang, W. Chu, Parametric analysis of the phase change material wall combining with micro-channel heat pipe and sky radiative cooling technology, Renew. Energy 178 (2021) 1057–1069.
[22] Y. Zhang, J. Ji, Z. Song, W. Ke, H. Xie, Performance prediction on a novel dual-mode heat pump with a hybrid photovoltaic/micro-channel heat pipe/fin heat exchanger, Energy Convers. Manag. 293 (2023) 117505.
[23] Z. Liu, Z. Quan, Y. Zhao, W. Zhang, M. Yang, J. Shi, Thermal performance analysis of ice thermal storage device based on micro heat pipe arrays: role of bubble-driven flow, Renew. Energy 217 (2023) 119151.
[24] Y. Guan, Q. Meng, T. Ji, W. Hu, W. Li, T. Liu, Experimental study of the thermal characteristics of a heat storage wall with micro-heat pipe array (MHPA) and PCM in solar greenhouse, Energy 264 (2023) 126183.
[25] T. Xiong, G. Liu, S. Huang, G. Yan, J. Yu, Two-phase flow distribution in parallel flow mini/micro-channel heat exchangers for refrigeration and heat pump systems: a comprehensive review, Appl. Therm. Eng. 201 (2022) 117820.
[26] S. Alfarawi, R. Al-Dadah, S. Mahmoud, Potentiality of new miniature-channels Stirling regenerator, Energy Convers. Manag. 133 (2017) 264–274.

[27] Z. Li, Y. Haramura, D. Tang, C. Guo, Analysis on the heat transfer characteristics of a micro-channel type porous-sheets Stirling regenerator, Int. J. Therm. Sci. 94 (2015) 37–49.
[28] B. Rutczyk, I. Szczygieł, A. Kabaj, Evaluation of an α type Stirling engine regenerator using a new differential model, Energy 209 (2020) 118369.
[29] H. Wang, B. Zhang, M. Liu, Z. Rao, Analytical solution of heat transfer performance of pin-array stack regenerator in Stirling cycle, Int. J. Therm. Sci. 167 (2021) 107015.
[30] S.C. Costa, H. Barrutia, J.A. Esnaola, M. Tutar, Numerical study of the pressure drop phenomena in wound woven wire matrix of a Stirling regenerator, Energy Convers. Manag. 67 (2013) 57–65.
[31] G. Xiao, H. Peng, H. Fan, U. Sultan, M. Ni, Characteristics of steady and oscillating flows through regenerator, Int. J. Heat Mass Transf. 108 (2017) 309–321.
[32] M. Ni, H. Peng, U. Sultan, K. Luo, G. Xiao, A quantitative method to describe the flow characteristics of an oscillating flow including porous media, Int. J. Heat Mass Transf. 119 (2018) 860–866.
[33] W.-L. Chen, K.-L. Wong, H.-E. Chen, An experimental study on the performance of the moving regenerator for a γ-type twin power piston Stirling engine, Energy Convers. Manag. 77 (2014) 118–128.
[34] Z. Buliński, A. Kabaj, T. Krysiński, I. Szczygieł, W. Stanek, B. Rutczyk, L. Czarnowska, P. Gładysz, A Computational Fluid Dynamics analysis of the influence of the regenerator on the performance of the cold Stirling engine at different working conditions, Energy Convers. Manag. 195 (2019) 125–138.
[35] Z. Li, Y. Haramura, Y. Kato, D. Tang, Analysis of a high performance model Stirling engine with compact porous-sheets heat exchangers, Energy 64 (2014) 31–43.
[36] D.D. Dai, F. Yuan, R. Long, Z.C. Liu, W. Liu, Imperfect regeneration analysis of Stirling engine caused by temperature differences in regenerator, Energy Convers. Manag. 158 (2018) 60–69.
[37] F. Xin, Z. Liu, S. Wang, W. Liu, Study of heat transfer in oscillatory flow for a Stirling engine heating tube inserted with spiral spring, Appl. Therm. Eng. 143 (2018) 182–192.
[38] S.C. Costa, I. Barreno, M. Tutar, J.A. Esnaola, H. Barrutia, The thermal non-equilibrium porous media modelling for CFD study of woven wire matrix of a Stirling regenerator, Energy Convers. Manag. 89 (2015) 473–483.
[39] M. Yu, C. Shi, Z. Liu, W. Liu, Design and multi-objective optimization of a new annular constructal bifurcation Stirling regenerator using response surface methodology, Int. J. Heat Mass Transf. 195 (2022).
[40] I. Urieli, D.M. Berchowitz, Stirling Cycle Engine Analysis, Adam Hilger LTD, Bristol, 1984.
[41] M. Tutar, A. Holdø, Computational modelling of flow around a circular cylinder in sub-critical flow regime with various turbulence models, Int. J. Numer. Methods Fluids 35 (7) (2001) 763–784.
[42] D. Gedeon, J.G. Wood, Oscillating-flow regenerator test rig: hardware and theory with derived correlations for screens and felts, NASA CR-198442, 1996.
[43] M. Chahartaghi, M. Sheykhi, Energy and exergy analyses of beta-type Stirling engine at different working conditions, Energy Convers. Manag. 169 (2018) 279–290.
[44] M.H. Ahmadi, M.-A. Ahmadi, F. Pourfayaz, Thermal models for analysis of performance of Stirling engine: a review, Renew. Sust. Energ. Rev. 68 (2017) 168–184.
[45] H. Hosseinzade, H. Sayyaadi, M. Babaelahi, A new closed-form analytical thermal model for simulating Stirling engines based on polytropic-finite speed thermodynamics, Energy Convers. Manag. 90 (2015) 395–408.
[46] R. Li, L. Grosu, D. Queiros-Condé, Losses effect on the performance of a Gamma type Stirling engine, Energy Convers. Manag. 114 (2016) 28–37.
[47] R.M. Wi'liam, Stirling Engine Design Manual: Second Edition, Prepared for National Aeronautics and Space Lewis Research Center under Grant NSG3194, DOE/NASA/3194–1 NASA CR-168088, 1983.
[48] K. Nilpueng, H.S. Ahn, D.-W. Jerng, S. Wongwises, Heat transfer and flow characteristics of sinusoidal wavy plate fin heat sink with and without crosscut flow control, Int. J. Heat Mass Transf. 137 (2019) 565–572.